ACS APPLIED MATERIALS & INTERFACES

Research Article

Cite This: ACS Appl. Mater. Interfaces XXXX, XXX, XXX−XXX

www.acsami.org

Bioinspired Mineralization with Hydroxyapatite and Hierarchical Naturally Aligned Nanofibrillar Cellulose

Yipin Qi,[†,∥,#] Zheng Cheng,[§,#] Zhou Ye,[†,‡] Hongli Zhu,[*,§] and Conrado Aparicio[*,†,‡]

[†]MDRCBB-Minnesota Dental Research Center for Biomaterials and Biomechanics and [‡]Department of Restorative Sciences, School of Dentistry, University of Minnesota, Minneapolis, Minnesota 55455, United States

[§]Department of Mechanical and Industrial Engineering, Northeastern University, Boston, Massachusetts 02115, United States

[∥]Department of Operative Dentistry and Endodontics, Guanghua School of Stomatology, Hospital of Stomatology, Guangdong Key Laboratory of Stomatology, Sun Yat-sen University, Guangzhou 510000, China

ABSTRACT: We used cellulose and a nonclassical mineralization process to fabricate a bioinspired nanohybrid material that exhibited structural features and properties similar to those of human hard tissues. We made a hydrogel with highly compacted and aligned cellulose nanofibers. We thoroughly mineralized the cellulose hydrogel with hydroxyapatite nanocrystals, using poly(acrylic acid) as a soluble template for precursor minerals, which infiltrated the nanocompartments of the aligned cellulose nanofiber network. The ultrastructure and mechanical properties of the mineralized gels were strikingly similar to those of bone and dentin, which supports further use of cellulose-based fibrillary materials as affordable, biocompatible scaffolds for repair and regeneration of hard tissues. The versatility of the bioinspired mineralization processes used here can broaden the applications of these cellulosic nanohybrids.

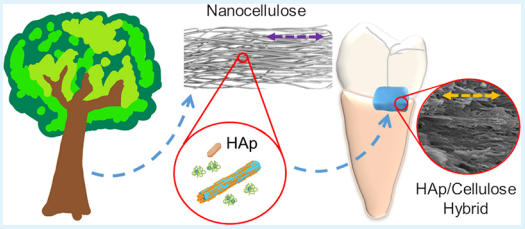

KEYWORDS: *nanocellulose, biomineralization, hydroxyapatite, biomimetic, dentin*

1. INTRODUCTION

Scaffolds for repairing and regenerating human hard tissue defects should mimic the chemical, structural, and mechanical properties of natural bone/dentin and have appropriate biochemical and nano/micro topographical features to trigger positive cell and tissue responses.[1] The basic building block of bone and dentin is a mineralized nanostructure of collagen fibrils that are interpenetrated and surrounded by platelets of hydroxyapatite (HAp) nanocrystals. Nanoscale replication of the hierarchical nanoapatite assembly within the collagen fibril has been proven to contribute to the mechanical properties of biomimetic scaffolds and to be critical to the ability of the matrix to confer key biological properties, including cell proliferation and differentiation, formation of focal adhesions by cells, and cytoskeletal arrangement.[2] Thus, biomimetic mineralization of the nanofibers, which mimics the chemical components and hierarchical structure of bone and dentin in micro and nanoscales, can produce an ideal candidate hybrid material for the repair and/or regeneration of damaged bones and/or teeth.[3]

Various natural or synthetic polymer-based composites/hybrids, that is, HAp-mineralized biopolymers, including collagen matrix, poly(lactic acid) (PLA), poly(glycolic acid) (PGA), poly(lactic acid-*co*-glycolic acid) (PLGA), poly(ε-caprolactone) (PCL), chitosan, and elastin-like polypeptides, have been developed[3−9] with biomimetic hierarchical structures and unique mechanical properties. However, a hybrid material that incorporates nano and microstructural features of the extracellular matrix, with mechanical properties resembling those of natural hard tissues, and biocompatible, affordable, and readily available biopolymers has not been achieved to date. The use of cellulose and other nature-derived polymers presents an opportunity to develop these challenging biocomposites due to the wide array of manufacturing methods for these polymers as well as the variety of organisms from which they can be sourced.

Cellulose is a naturally occurring polymer with outstanding mechanical properties. Cellulose also exhibits excellent biocompatibility, abundance, biodegradability, nontoxicity, low-cost, and accessibility as it can be extracted from lignocellulosic biomass or synthesized from specific bacteria.[10−12] The use of cellulose as a base component for fabricating hydrogels and other constructs for biomedical applications has gained significant attention.[13] The functional groups in the backbone of cellulose and its derivatives have been used to manufacture biocompatible hydrogels with unique structures and multiple functionalities that enable their use in biomedical applications. However, the mechanical properties of nanocellulose hydrogels are limited, impeding their applicability in hard tissue regeneration. To overcome the low mechanical properties of cellulose scaffolds as well as to improve the bioactive properties for hard tissue regeneration, mineralization of cellulose hydrogels with HAp and other calcium phosphates has been actively investigated in recent

Received: May 30, 2019
Accepted: July 14, 2019
Published: July 15, 2019

DOI: 10.1021/acsami.9b09443
ACS Appl. Mater. Interfaces XXXX, XXX, XXX−XXX

years.[14−21] For most of these studies, either simulated body fluids or other supersaturated solutions of Ca^{2+} and PO_4^{3-} were used as ionic sources for the nucleation and growth of calcium phosphate minerals on insoluble cellulose matrices. The minerals produced using these mineralizing solutions were deposited on or near to the surface of the cellulose matrix, forming microstructural aggregates of HAp nanocrystals. The resultant nanostructure of the nanocellulose/HAp hybrids are notably different from that of natural hard tissues and have relatively lower hardness.[22]

During mineralization of the extracellular matrix of hard tissues in nature, insoluble collagen fibrils act as a structural template in which the interstices inside the fibrils serve as confined nanocompartments for mineral deposition.[23] Thorough intrafibrillar mineralization of the structural matrix can be obtained in vitro using biomimetic methods. Polyanions stabilize prenucleation clusters that bind to and infiltrate the fibrillar collagen and subsequently transform into amorphous calcium phosphate and, finally, crystalline HAp with their [001] direction parallel to the long axes of the collagen fibrils as in the case of bone.[24,25] Poly(aspartic acid), poly(acrylic acid), and even some polycations have been used in in vitro biomimetic models as soluble active templates for collagen mineralization. However, few biopolymer-based fibrillary structures other than collagen have been biomineralized with HAp using this or similar biomimetic processes.[6] The presence of nanocompartments in the structural matrix seems to be necessary for facilitating the penetration of the polyanion-stabilized amorphous clusters and confining the minerals inside the insoluble templating structure during transformation into the stable crystalline phase.[23,26] This has limited the applicability of polymeric structures as alternative organic matrices in directing mineralization using processes that mimic the one for mineralizing collagen. Molecular self-assembly of the polymers that form the scaffold, such as those in collagen and elastin polymers,[6,23] or controlled dense compaction of the fibrils in the structure, as we have done here, can be exploited to provide the necessary nanocompartments and enable mineralization. In this work, we fabricated a bioinspired hybrid hydrogel made of highly compacted and aligned cellulose nanofibers that was thoroughly mineralized with embedded HAp nanocrystals. The obtained bioinspired hybrids exhibited structural features and properties similar to those of human hard tissues.

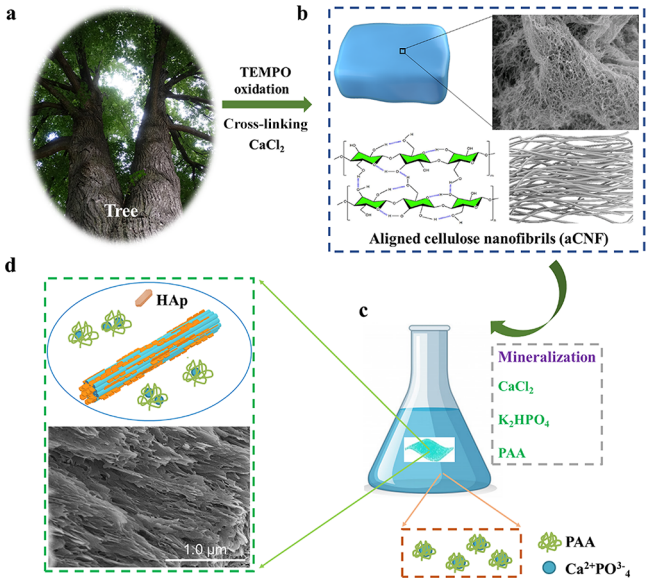

Figure 1. Schematics of fabrication of the m-aCNF composite. (a) Tree. (b) aCNF and its structure. (c) Mineralization process. (d) Obtained m-aCNF material and its SEM micrograph, showing an aligned mineralized structure.

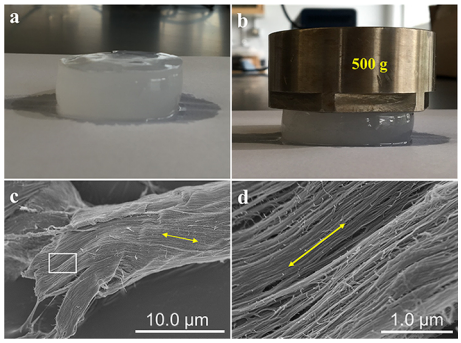

Figure 2. Photographs and SEM micrographs of aCNF hydrogels. (a) 50 mm diameter hydrogel sample. (b) Same cellulose gel sample with a loaded weight of 500 g. The hydrogel maintained its structural integrity and did not collapse. (c) SEM image of an aCNF fiber before mineralization. (d) Magnified SEM image of the aCNF fiber from the area marked with a rectangle in (c). The yellow arrows in (c) and (d) indicate the well-aligned cellulose nanofibers.

2. RESULTS AND DISCUSSION

Nature-derived wood fiber has a hierarchical structure with one large microfiber composed of thousands of aligned nanofibers (Figure 1a,b). In this work, we fabricated a hydrogel made of cellulose microfibers that were treated by (2,2,6,6-tetramethyl-1-piperidinyloxy) TEMPO-mediated oxidation and modest physical sonication. The C6 hydroxyl groups of the cellulose chain were partially oxidized to carboxyl groups, which have a lower zeta potential. During the fabrication process, the positive Ca^{2+} was used as a cross-linker between the negative carboxyl and hydroxyl groups on the cellulose chains, which significantly promoted gelation of the oxidized fibers, stabilizing their 3D structure.[27,28] The hydrogel after $CaCl_2$ treatment was transparent and mechanically strong (Figure 2a,b). There were still highly aligned cellulose nanofibers (aCNF) inside the individual microfiber (Figure 1b). In this work, we used the biomimetic mineralization process (Figure 1c) with $CaCl_2$, K_2HPO_4, and poly(acrylic acid) (PAA) to mineralize the aCNF, and thus, we obtained the fully mineralized aCNF (m-aCNF) composite (Figure 1d).

Visualization by scanning electron microscopy (SEM) of the aCNF hydrogels revealed that these gels contained fibers of ∼8−10 μm in diameter (Figure 2c), which were composed of aligned nanocellulose fibril bundles (∼20 nm diameter) (Figure 2d). This occurred because the microfiber is corrupted and partially disintegrated by TEMPO oxidation treatment and moderate sonication.[29] However, the aligned nanofibers inside the microfiber remained unchanged. The alignment of the nanofibrils in the hydrogel is a preservation of the natural alignment in the cellulose as imparted by the plant cell wall from which it was derived. The alignment of the nanofibers generated a highly compacted fibrillary nanostructure in the aCNF gels with spaces between nanofibers of smaller dimensions than the diameter of the nanofibers.

After 28 days of immersion in the biomimetic mineralizing solution (4.5 mM $CaCl_2$, 4.2 mM K_2HPO_4, 50 mg/L, 450 kDa

DOI: 10.1021/acsami.9b09443
ACS Appl. Mater. Interfaces XXXX, XXX, XXX−XXX

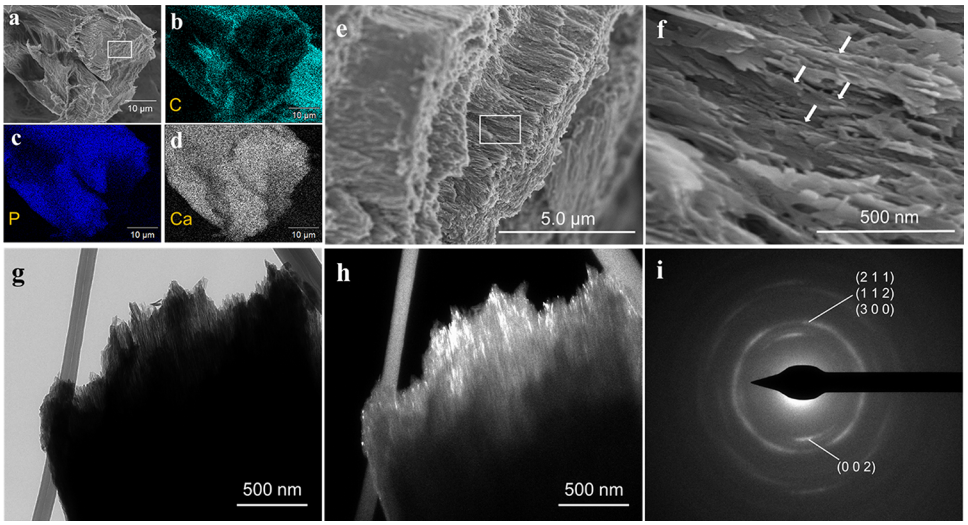

Figure 3. Elemental analysis, SEM, and TEM micrographs of mineralized cellulose gels. (a–d) Cross-sectional SEM images and elemental mappings of the m-aCNF after 28 days of mineralization in the PAA mineralizing solution. (e, f) SEM images from the marked area in (a) and (e), respectively. The arrows indicate the aligned mineral nanocrystals withthe direction of the nanofibers. (g, h) Bright-field and dark-field TEM micrographs showed high infiltration of aligned nanocrystals in the cellulose fibrils. (i) SAED analysis of the obtained nanocrystals showed characteristic patterns of oriented HAp with arcing of the (002) plane.

PAA), the aCNF hydrogels were fully mineralized with a continuous network of minerals throughout the full section of the m-aCNF fibers. Twenty-eight days was the minimum period needed to obtain the m-aCNF gels. The minerals were tightly packed and thoroughly infiltrated the cellulose nanofiber bundles (Figures 1d and 3a,e). PAA has been used as an analog of noncollagenous proteins in in vitro biomimetic models for collagen mineralization to develop biomimetic scaffolds and constructs for bone and dentin tissue engineering. We used 50 mg/L of PAA with a molecular weight of 450 kDa as these are the optimal conditions for obtaining effective and fast (i.e., within 1 day in solution) intrafibrillar mineralization of collagen gels.[30] PAA has dual functions: it acts as both an inhibitor and a promoter of mineralization in these in vitro mineralizing systems.[31] PAA molecular weight and concentration modulate the infiltration of the polymeric matrix by (i) providing solution stability (inhibition effect), that is, preventing spontaneous precipitation of HAp crystals and/or extrafibrillar mineralization of the polymer matrix and (ii) control over the number and growth of the PAA-stabilized mineral precursors that formed in solution (promoter effect) before entering the polymer matrix.[30,31] A wide range of combinations of PAA molecular weight and concentration enable intrafibrillar mineralization of collagen[30] and the same was expected for mineralization of our m-aCNF material. Even though the PAA molecular weight and concentration we used might not be optimal for mineralizing aCNF hydrogels, these PAA properties proved to be in the appropriate range to obtain thorough mineralization.

The nanostructure of m-aCNF contained platelet-like nanocrystals of ~100 nm in length and ~50 nm in width, as visualized in SEM micrographs of the cross section of m-aCNF fibers (Figure 3f). The crystals were aligned and packed along the cellulose nanofibers (Figure 3f, arrows). The alignment and infiltration were further confirmed by transmission electron microscopy (TEM) micrographs. Cross-sectional view of an m-aCNF fiber (Figure 3g) showed nanocrystals throughout the entire bundle of nanofibers. Dark-field TEM micrographs for the (002) plane also showed thorough infiltration of aligned crystals (Figure 3h).

Further characterizations of the chemistry and structure of aCNF and m-aCNF materials, including energy-dispersive X-ray spectroscopy (EDS), selected area electron diffraction (SAED), X-ray diffraction (XRD), and attenuated total reflectance-Fourier transform infrared spectroscopy (ATR-FTIR) confirmed the existence of carbonated HAp nanocrystals within the cellulose fibers of the m-aCNF gels.

C, Ca, and P elemental mappings by EDS confirmed the thorough mineralization throughout the nanofiber bundle (Figure 3a–d). The Ca/P ratio was 1.53 for the area analyzed, which was slightly lower than that of the stoichiometric HAp (1.67). This low Ca/P ratio suggested that the HAp minerals in m-aCNF were Ca-deficient, as is the case for the carbonated calcium-deficient HAp found in natural hard tissues (1.51–1.64).[32,33]

We confirmed that the crystals infiltrating the m-aCNF gels were HAp by XRD (Figure 4a), ATR-FTIR (Figure 4b), and SAED (Figure 3i). XRD patterns of nonmineralized aCNF

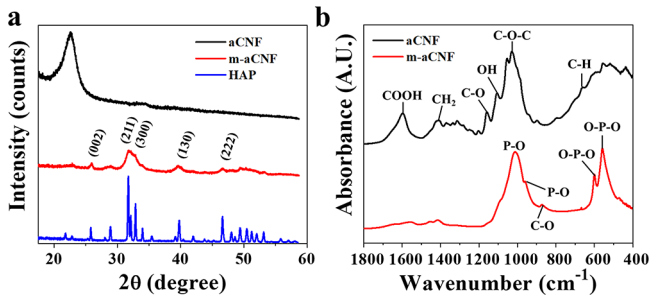

Figure 4. Characterization of cellulose nanofibers before (aCNF) and after mineralization (m-aCNF) in a PAA-containing mineralizing solution. (a) XRD spectra of m-aCNF (red) showed characteristic peaks of HAp from the (002), (211), (300), (130), and (222) planes, nonmineralized aCNF (black), and HAp disk (blue). (b) ATR-FTIR spectra for aCNF (black) and m-aCNF (red) gels with labeled characteristic peaks of cellulose and carbonated HAp, respectively.

DOI: 10.1021/acsami.9b09443
ACS Appl. Mater. Interfaces XXXX, XXX, XXX–XXX

displayed a characteristic native cellulose peak with broad diffraction at approximately 2θ = 22.6°, which indicated a crystalline structure with (200) plane of cellulose I.[34,35] XRD pattern of m-aCNF included peaks for the HAp (002), (211), (300), (130), and (222) planes. The XRD peaks for mineralized cellulose gels were broader than the peaks of the same planes for pure HAp, which is most likely due to the nanosize nature of the HAp crystals in m-aCNF gels (Figure 3f–h). ATR-FTIR spectra for aCNF gels had characteristic adsorption bands of cellulose, that is, the C–O antisymmetric bridge stretching, –OH skeletal vibration, C–O–C pyranose ring skeletal vibration, CH_2 symmetric bending, out-of-plane deformation of the C–H functional group, and asymmetrical carboxylate COO^- vibration.[34,36] The adsorption bands for the characteristic phosphate (556 and 600 cm^{-1}) and carbonate (870 cm^{-1}) groups of carbonated HAp[37] were prominent in the spectra for m-aCNF materials. The major characteristic bands for P–O bonds in HAp at 958 and 1020 cm^{-1} were overlapped with the bands for the C–O–C groups of the cellulose matrix. SAED analysis of the crystals also displayed the characteristic HAp patterns with arcing of the (002) planes, indicating that the HAp nanocrystals were aligned in the [001] direction parallel to the longitudinal axis of the cellulose fibrils (Figure 3i). The oriented hybrid nanostructure in m-aCNF was strikingly similar to the ultrastructure of natural organic–inorganic hybrid composites with unique hierarchical structures like bone and dentin.[38] CNF gels manufactured with an analogous process but without alignment of the cellulose nanofibers were also mineralized, but thorough infiltration of the cellulose fiber bundles and mineral orientation along the fibers were not achieved (Figure 5).

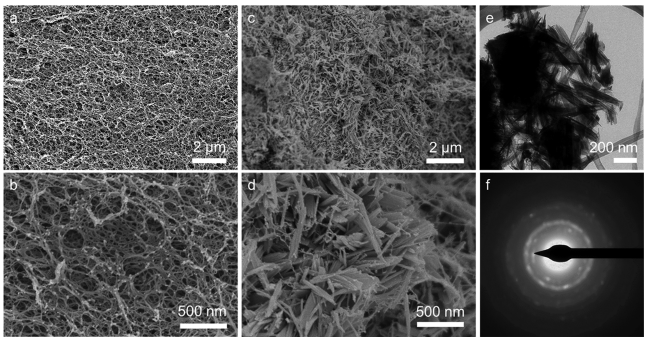

Figure 5. SEM and TEM micrographs of gels made of nonaligned cellulose nanofibers before and after mineralization. (a, b) Cross-sectional SEM images. (c, d) SEM images of materials with nonaligned cellulose fibers after 28 days of mineralization in the PAA mineralizing solution. (e) Bright-field TEM micrograph showing randomly oriented mineral crystals. (f) SAED analysis of the obtained nanocrystals showing multiple arcs for the (002) plane.

Thus, the alignment of cellulose nanofibers in aCNF hydrogels appeared to be a key structural feature in the successful and thorough infiltration of minerals in the m-aCNF materials when using PAA as the mineral precursor stabilizer. The much smaller and aligned nanospaces of the aCNF gels in comparison to nonaligned CNF gels might play an analogous role in intrafibrillar mineralization of m-aCNF to that of gap zones in self-assembled fibrillary collagen structures in natural hard tissues. Nanocompartments also play a critical role during biomimetic intrafibrillar mineralization of synthetic collagen fibrillary structures and self-assembled fibers of elastin-like recombinant polymers.[6]

Thermogravimetric analysis (TGA) confirmed that the m-aCNF composite contained large amounts of minerals. The m-aCNF composite showed higher thermal stability during TGA experiments than nonmineralized aCNF (Figure 6). Most of

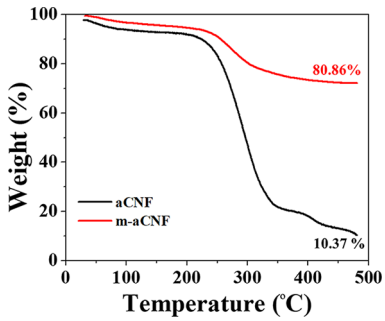

Figure 6. Thermogravimetric analysis of m-aCNF and aCNF materials. Values on each curve represent the percentage of weight sample remaining after competition of thermal disintegration.

the mass loss in both samples occurred at the 225–350 °C heating range due to the thermal degradation and burn out of cellulosic polysaccharide. The aCNF gels also lost notable mass content due to degradation of the remaining organic material (oxygen-containing groups, that is, hydroxyl, carboxyl, and ether groups) into carbon residues between 350–480 °C.[39] Two exothermic reactions occurred, which were attributed to active flaming combustion and char oxidation.[36,40] These carbon residues seemed to be stabilized by the minerals in m-aCNF samples and thus were not significantly degraded in this range of temperatures. The final remaining contents (mostly mineral in m-CNF but also salts and organic residues) at 480 °C were 80.86 and 10.37 wt % for m-aCNF and aCNF, respectively. The roughly 70 wt % mineral content in m-aCNF samples is, once again, comparable with the mineral content in natural hard tissues (ranging ~70–85 wt %)[41] and other HAp-mineralized fibrillary synthetic collagen and elastin-based materials.[30,42,43]

The highly ordered and highly mineralized structure of intrafibrillar mineralization at the nanoscale is considered to be the foundation of biomechanical properties of natural hard tissues.[44,45] We determined elastic modulus and hardness of the m-aCNF nanohybrid structures by nanoindentation. We assessed that the mechanical properties of our mineralized cellulose-based hybrids after rehydration, that is, close to natural conditions, were comparable to those of mouse cortical bone and human dentin (Figure 7). The nanomechanical test of different kinds of CNF samples is illustrated in Figure 7a. Meanwhile, the representative nanoindentation load–displacement curves are shown in Figure 7b. Values of elastic modulus in a dry state for dentin and cortical bone were significantly higher than those for m-aCNF samples, although in the same order of magnitude (Figure 7c,e). Cortical bone hardness in a dry state was also significantly higher than dentin and m-aCNF hardness (Figure 7d,f). However, when all materials were tested and compared in rehydrated conditions, the natural hard tissues and m-aCNF hybrids displayed mechanical properties with no significant differences. Similarly, we have reported that in vitro intrafibrillarly mineralized collagen membranes in dry and rehydrated states have higher and lower mechanical properties, respectively, than m-aCNF.[46] The greater effect of

DOI: 10.1021/acsami.9b09443
ACS Appl. Mater. Interfaces XXXX, XXX, XXX–XXX

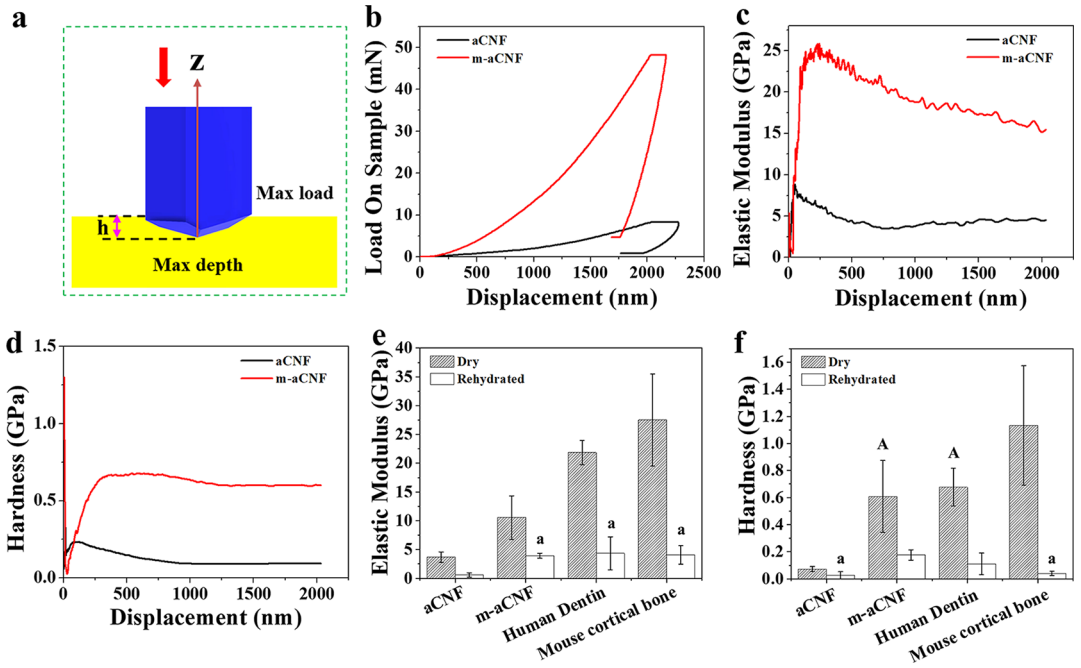

Figure 7. Mechanical properties of aCNF, m-aCNF, and natural tissues (mouse cortical bone and human dentin) in dry and rehydrated states. (a) Schematic illustration of the nanoindentation test process. Representative (b) nanoindentation load−displacement, (c) elastic modulus, and (d) hardness vs penetration depth of the indenter curves for aCNFs (black) and m-aCNFs (red) samples in dry state. (e) Elastic modulus and (f) hardness of aCNF, m-aCNF, human dentin, and mouse cortical bone in dry and rehydrated states. Values with "a" or "A" had no statistically significant differences in dry or rehydrated state, respectively.

water on lowering mechanical properties of hard tissues and in vitro intrafibrillarly mineralized collagen membranes than of m-aCNF hybrids might be associated with a notably lower incorporation of water into m-aCNF than collagen-based mineralized materials. The more compact cellulose fiber bundles (~10 μm in diameter) than reconstituted collagen fibers (100−200 nm in diameter) might leave less space for water infiltration after mineralization. The similar nanostructure and mechanical properties of m-aCNF hybrids and natural hard tissues in hydrated conditions support further use of cellulose-based fibrillary materials as affordable, versatile, and biocompatible scaffolds for repair and regeneration of hard tissues.

3. CONCLUSIONS

In the present study, TEMPO-oxidized cellulose hydrogels with highly compact and well-aligned nanofibers were fabricated and mineralized with HAp crystals using a biomimetic method to obtain a hybrid nanocomposite with nanostructural features (composition, distribution, structure, orientation of crystals) and mineral content resembling those of natural hard tissues. The exceptional mechanical properties (elastic modulus and hardness) of m-aCNF nanohybrids were comparable to those of natural hard tissues, including human dentin and mouse cortical bone, in hydrated conditions. Thus, this nanocellulose-based biohybrid is a promising candidate material for hard tissue repair and regeneration. The versatility in the fabrication methods of cellulose could be utilized to tailor the structure and properties of hybrid cellulosic materials. Similarly, the bioinspired mineralization processes, such as the use of soluble templates to stabilize mineral precursors, may be used to produce cellulose-based hybrids with high contents of minerals other than HAp.[47−49] The latter might expand the use of cellulosic nanohybrids beyond biomedicine.

4. EXPERIMENTAL SECTION

4.1. Fabrication of aCNF Hydrogel. Nanofibrillar cellulose hydrogel with a cellulose weight percentage of 1.44 was prepared from softwood pulp. First, 2 g of dry weight softwood pulp was added to 100 mL of DI water containing 0.032 g of TEMPO, 0.2 g of NaBr, and 6 mL of 12.5 wt % NaClO solution (Sigma-Aldrich, St. Louis, MO, USA). NaOH (0.5 M) was added to maintain a pH = 10.5 at ambient temperature. After 2 h, the pH of the resulting mixture showed no further change, and the reaction was terminated. The oxidized cellulose fibers dispersion was immersed in a 0.1 M $CaCl_2$ solution in a mold and sonicated for 10 min to initiate gelation. Finally, the gel precursor was left to stand at room temperature for 24 h to obtain well-formed hydrogels. The resulted cellulose hydrogel was gently taken out and washed with DI water.

4.2. Mineralization of aCNF. $CaCl_2$ (9 mM) and 4.2 mM K_2HPO_4 (Sigma-Aldrich, St. Louis, MO, USA) solutions were prepared in a Tris-buffered saline (TBS) at pH 7.4 and 37 °C. PAA with a molecular weight of 450 kDa (Sigma-Aldrich, St. Louis, MO, USA) was used as a mineralizing agent and dissolved in a phosphate solution of 100 mg/L before being mixed with an equal volume of calcium counterion solution. Thus, a mineralization solution of PAA (450 kDa) at 50 mg/L concentration was prepared. Cellulose hydrogels were cut into 5 × 5 × 5 mm cubes and incubated in the aforementioned mineralizing solution[25] at 37 °C with agitation. Mineralizing solutions were refreshed every 3 days. After 28 days, the cellulose hydrogel cubes were collected and rinsed with DI water twice. Cellulose hydrogel cubes were dried with serial dehydration in ethanol and critical point drying (Samdri-780A, tousimis, Rockville, MD, USA) for further characterization with nonmineralized specimens.

4.3. Scanning Electron Microscopy (SEM) and Transmission Electron Microscopy (TEM). The morphologies of the specimens were imaged with a field emission gun SEM (Hitachi SU8230, Tokyo, Japan) operated at an accelerating voltage of 3 kV. All specimens were

DOI: 10.1021/acsami.9b09443
ACS Appl. Mater. Interfaces XXXX, XXX, XXX−XXX

sputter-coated with a 5 nm-thick iridium layer. For elemental analysis of the mineralized samples, energy-dispersive X-ray spectroscopy (EDS) analysis was performed during SEM examination.

Mineralized cellulose hydrogels were crushed into fine-grained powders in liquid nitrogen, dispersed in ethanol, and dropped on a lacey carbon-coated Nickel TEM grid with a 200 mesh size. Samples were analyzed using a TEM (FEI Tecnai G2 Spirit BioTWIN, Thermo Fisher Scientific, Waltham, MA, USA) operated at 120 kV in bright-field (BF), dark-field (DF), and selected area electron diffraction (SAED) modes.

4.4. Attenuated Total Reflectance-Fourier Transform Infrared Spectroscopy (ATR-FTIR). FTIR analysis of the dried aCNF gel and m-aCNF hybrid was performed using an FTIR spectrometer (Nicolet iS50, Thermo Fisher Scientific, Waltham, MA, USA), equipped with a built-in diamond attenuated total reflection (ATR) for single-spot ATR measurement. Each spectrum was the result of signal-averaging of 32 scans at a resolution of 2 cm^{-1} with a wavenumber range of 400 to 4000 cm^{-1}.

4.5. X-ray Diffraction (XRD). The crystal structure of aCNF, m-aCNF, and HAp disks was characterized using a microdiffractometer system with a two-dimensional area detector (AXS, Bruker, Billerica, MA, USA) operated at 40 kV and 35 mA. The detector covered the angular range 2θ of 17.5 to 60°. The data was collected with two frames per collection time and 1500 s for each frame. The results were analyzed using JADE8 software (Materials Data Inc., JADE, Livermore, CA, USA).

4.6. Thermogravimetric Analysis (TGA). The thermal behavior of the dried cellulose samples before and after mineralization was measured using a 409 PC (Netzsch STA, Selb, Germany). The samples were heated under a nitrogen atmosphere from room temperature up to 480 °C at a heating rate of 10 °C min^{-1}.

4.7. Nanoindentation. Mechanical properties of the aCNF and m-aCNF samples were examined using a nanoindentor (XP, MTS Systems Corporation, Eden Prairie, MN, USA) equipped with a Berkovich tip at room temperature. TestWorks 4 software (MTS Systems Corporation, Eden Prairie, MN, USA) was used to analyze the elastic modulus and hardness. The dried aCNF, m-aCNF, human dentin, and mouse cortical bone were embedded in epoxy resin, sectioned to reveal an indentation surface and polished with polishing papers (SiC; 600, 800, and 1200) and alumina slurries (1, 0.3, and 0.05 μm). Cortical bone samples were obtained by sectioning the midshaft of one femur from a healthy wild type 9-week-old male mouse (courtesy of Professor Lincoln Potter, University of Minnesota, IACUC exempt). The human dentin samples were obtained from a pull of unidentified third molars with no apparent signs of decay that were extracted at the University of Minnesota, School of Dentistry Clinics (IRB exempt). The roots were removed from the crown and then cut perpendicularly to their longitudinal axis at the middle third from the crown. A total of at least seven indents were performed on the specimen surfaces. The maximum indentation depth was set at 2000 nm. For the rehydrated specimens, the embedded specimens were rehydrated in DI water overnight and covered with a piece of soaked tissue before the tests. Sectioned surfaces were kept wet, and at least seven indents were ran for each sample during nanoindentation tests. The Oliver–Pharr data analysis method was used to analyze the elastic modulus and hardness at the depth of 2000 nm. Analysis of the statistically significant differences on mechanical properties among groups was performed with one-way ANOVA with Turkey's multiple comparison post-hoc test. The level of statistical significance was set at $p < 0.05$.

AUTHOR INFORMATION

Corresponding Authors

*E-mail: h.zhu@neu.edu (H.Z.).
*E-mail: apari003@umn.edu (C.A.).

ORCID

Zhou Ye: 0000-0003-4220-0919
Hongli Zhu: 0000-0003-1733-4333
Conrado Aparicio: 0000-0003-2969-6067

Author Contributions

#Y.Q. and Z.C. contributed equally to this work. This work was conceived by C.A. and H.Z., designed by C.A., H.Z., Y.Q., and Z.C., performed by Y.Q., Z.C., and Z.Y., and analyzed and written by all authors. All authors have given approval to the final version of the manuscript.

Notes

The authors declare no competing financial interest.

ACKNOWLEDGMENTS

H.Z. would like to thank the financial support from the Northeastern University. Parts of this work were carried out in the University of Minnesota I.T. Characterization Facility, which receives partial support from NSF through the MRSEC program. The authors thank David De Jong for editing the language of this paper.

REFERENCES

(1) Dimitriou, R.; Jones, E.; McGonagle, D.; Giannoudis, P. V. Bone Regeneration: Current Concepts and Future Directions. *BMC Med.* **2011**, DOI: 10.1186/1741-7015-9-66.

(2) Liu, Y.; Luo, D.; Kou, X.-X.; Wang, X.-D.; Tay, F. R.; Sha, Y.-L.; Gan, Y.-H.; Zhou, Y.-H. Hierarchical Intrafibrillar Nanocarbonated Apatite Assembly Improves the Nanomechanics and Cytocompatibility of Mineralized Collagen. *Adv. Funct. Mater.* **2013**, 1404.

(3) Li, Y.; Chen, X.; Fok, A.; Rodriguez-Cabello, J. C.; Aparicio, C. Biomimetic Mineralization of Recombinamer-Based Hydrogels toward Controlled Morphologies and High Mineral Density. *ACS Appl. Mater. Interfaces* **2015**, 25784.

(4) Lanao, R. P. F.; Jonker, A. M.; Wolke, J. G. C.; Jansen, J. A.; van Hest, J. C. M.; Leeuwenburgh, S. C. G. Physicochemical Properties and Applications of Poly(Lactic-Co-Glycolic Acid) for Use in Bone Regeneration. *Tissue Eng., Part B* **2013**, 380.

(5) Rezwan, K.; Chen, Q. Z.; Blaker, J. J.; Boccaccini, A. R. Biodegradable and Bioactive Porous Polymer/Inorganic Composite Scaffolds for Bone Tissue Engineering. *Biomaterials* **2006**, 3413.

(6) Li, Y.; Rodriguez-Cabello, J. C.; Aparicio, C. Intrafibrillar Mineralization of Self-Assembled Elastin-Like Recombinamer Fibrils. *ACS Appl. Mater. Interfaces* **2017**, 5838.

(7) Schneider, O. D.; Loher, S.; Brunner, T. J.; Uebersax, L.; Simonet, M.; Grass, R. N.; Merkle, H. P.; Stark, W. J. Cotton Wool-like Nanocomposite Biomaterials Prepared by electrospinning:In vitro bioactivity and Osteogenic Differentiation of Human Mesenchymal Stem Cells. *J. Biomed. Mater. Res., Part B* **2008**, 350.

(8) Chen, J.; Pan, P.; Zhang, Y.; Zhong, S.; Zhang, Q. Preparation of Chitosan/Nano Hydroxyapatite Organic-Inorganic Hybrid Microspheres for Bone Repair. *Colloids Surf., B* **2015**, 401.

(9) El-Fiqi, A.; Seo, S. J.; Kim, H. W. Mineralization of Fibers for Bone Regeneration. In *Biomineralization and Biomaterials: Fundamentals and Applications*; Woodhead Publishing: 2015, DOI: 10.1016/B978-1-78242-338-6.00016-8.

(10) Cheng, Z.; Yang, R.; Liu, X.; Liu, X.; Chen, H. Green Synthesis of Bacterial Cellulose via Acetic Acid Pre-Hydrolysis Liquor of Agricultural Corn Stalk Used as Carbon Source. *Bioresour. Technol.* **2017**, 8.

(11) Cheng, Z.; Ma, Y.; Yang, L.; Cheng, F.; Huang, Z.; Natan, A.; Li, H.; Chen, Y.; Cao, D.; Huang, Z.; Wang, Y.; Liu, Y.; Yang, R.; Zhu, H. Plasmonic-Enhanced Cholesteric Films: Coassembling Anisotropic Gold Nanorods with Cellulose Nanocrystals. *Adv. Opt. Mater.* **2019**, 1801816.

(12) Li, H.; Cheng, Z.; Zhang, Q.; Natan, A.; Yang, Y.; Cao, D.; Zhu, H. Bacterial-Derived, Compressible, and Hierarchical Porous Carbon for High-Performance Potassium-Ion Batteries. *Nano Lett.* **2018**, 7407.

DOI: 10.1021/acsami.9b09443
ACS Appl. Mater. Interfaces XXXX, XXX, XXX–XXX

(13) Fu, L. H.; Qi, C.; Ma, M. G.; Wan, P. Multifunctional Cellulose-Based Hydrogels for Biomedical Applications. *J. Mater. Chem. B* **2019**, 1541.
(14) Wan, Y. Z.; Hong, L.; Jia, S. R.; Huang, Y.; Zhu, Y.; Wang, Y. L.; Jiang, H. J. Synthesis and Characterization of Hydroxyapatite-Bacterial Cellulose Nanocomposites. *Compos. Sci. Technol.* **2006**, 1825.
(15) Busuioc, C.; Stroescu, M.; Stoica-Guzun, A.; Voicu, G.; Jinga, S.-I. Fabrication of 3D Calcium Phosphates Based Scaffolds Using Bacterial Cellulose as Template. *Ceram. Int.* **2016**, 15449.
(16) Duarte, E. B.; das Chagas, B. S.; Andrade, F. K.; Brígida, A. I. S.; Borges, M. F.; Muniz, C. R.; Souza Filho, M. de S. M.; Morais, J. P. S.; Feitosa, J. P. A.; Rosa, M. F. Production of Hydroxyapatite−bacterial Cellulose Nanocomposites from Agroindustrial Wastes. *Cellulose* **2015**, 3177.
(17) Torgbo, S.; Sukyai, P. Bacterial Cellulose-Based Scaffold Materials for Bone Tissue Engineering. *Appl. Mater. Today.* **2018**, 34.
(18) Salama, A. Cellulose/Calcium Phosphate Hybrids: New Materials for Biomedical and Environmental Applications. *Int. J. Biol. Macromol.* **2019**, 606.
(19) Abouzeid, R. E.; Khiari, R.; Beneventi, D.; Dufresne, A. Biomimetic Mineralization of Three-Dimensional Printed Alginate/TEMPO-Oxidized Cellulose Nanofibril Scaffolds for Bone Tissue Engineering. *Biomacromolecules* **2018**, 4442.
(20) Joshi, M. K.; Pant, H. R.; Tiwari, A. P.; Maharjan, B.; Liao, N.; Kim, H. J.; Park, C. H.; Kim, C. S. Three-Dimensional Cellulose Sponge: Fabrication, Characterization, Biomimetic Mineralization, and in Vitro Cell Infiltration. *Carbohydr. Polym.* **2016**, 154.
(21) Fragal, E. H.; Cellet, T. S. P.; Fragal, V. H.; Companhoni, M. V. P.; Ueda-Nakamura, T.; Muniz, E. C.; Silva, R.; Rubira, A. F. Hybrid Materials for Bone Tissue Engineering from Biomimetic Growth of Hydroxiapatite on Cellulose Nanowhiskers. *Carbohydr. Polym.* **2016**, 734.
(22) Reznikov, N.; Bilton, M.; Lari, L.; Stevens, M. M.; Kröger, R. Fractal-like Hierarchical Organization of Bone Begins at the Nanoscale. *Science* **2018**, eaao2189.
(23) Nudelman, F.; Pieterse, K.; George, A.; Bomans, P. H. H.; Friedrich, H.; Brylka, L. J.; Hilbers, P. A. J.; De With, G.; Sommerdijk, N. A. J. M. The Role of Collagen in Bone Apatite Formation in the Presence of Hydroxyapatite Nucleation Inhibitors. *Nat. Mater.* **2010**, 1004.
(24) Cölfen, H. A Crystal-Clear View. *Nat. Mater.* **2010**, 960.
(25) Jee, S. S.; Thula, T. T.; Gower, L. B. Development of Bone-like Composites via the Polymer-Induced Liquid-Precursor (PILP) Process. Part 1: Influence of Polymer Molecular Weight. *Acta Biomater.* **2010**, 3676.
(26) Niu, L. N.; Jee, S. E.; Jiao, K.; Tonggu, L.; Li, M.; Wang, L.; Yang, Y. D.; Bian, J. H.; Breschi, L.; Jang, S. S.; Chen, J. H.; Pashley, D. H.; Tay, F. R. Collagen Intrafibrillar Mineralization as a Result of the Balance between Osmotic Equilibrium and Electroneutrality. *Nat. Mater.* **2017**, 370.
(27) Yang, L.; Mukhopadhyay, A.; Jiao, Y.; Yong, Q.; Chen, L.; Xing, Y.; Hamel, J.; Zhu, H. Ultralight, Highly Thermally Insulating and Fire Resistant Aerogel by Encapsulating Cellulose Nanofibers with Two-Dimensional MoS2. *Nanoscale* **2017**, 11452.
(28) Cao, D.; Xing, Y.; Tantratian, K.; Wang, X.; Ma, Y.; Mukhopadhyay, A.; Cheng, Z.; Zhang, Q.; Jiao, Y.; Chen, L.; Zhu, H. 3D Printed High-Performance Lithium Metal Microbatteries Enabled by Nanocellulose. *Adv. Mater.* **2019**, 1807313.
(29) Dippold, D.; Cai, A.; Hardt, M.; Boccaccini, A. R.; Horch, R.; Beier, J. P.; Schubert, D. W. Novel Approach towards Aligned PCL-Collagen Nanofibrous Constructs from a Benign Solvent System. *Mater. Sci. Eng. C* **2017**, 278.
(30) Qi, Y.; Ye, Z.; Fok, A.; Holmes, B. N.; Espanol, M.; Ginebra, M. P.; Aparicio, C. Effects of Molecular Weight and Concentration of Poly(Acrylic Acid) on Biomimetic Mineralization of Collagen. *ACS Biomater. Sci. Eng.* **2018**, 2758.
(31) Huang, S.-C.; Naka, K.; Chujo, Y. Effect of Molecular Weights of Poly(Acrylic Acid) on Crystallization of Calcium Carbonate by the Delayed Addition Method. *Polym. J.* **2008**, 154.
(32) Kuhn, L. T.; Grynpas, M. D.; Rey, C. C.; Wu, Y.; Ackerman, J. L.; Glimcher, M. J. A Comparison of the Physical and Chemical Differences between Cancellous and Cortical Bovine Bone Mineral at Two Ages. *Calcif. Tissue Int.* **2008**, 146.
(33) Rythén, M.; Sabel, N.; Dietz, W.; Robertson, A.; Norén, J. G. Chemical Aspects on Dental Hard Tissues in Primary Teeth from Preterm Infants. *Eur. J. Oral Sci.* **2010**, 389.
(34) Zhao, Y.; Moser, C.; Lindström, M. E.; Henriksson, G.; Li, J. Cellulose Nanofibers from Softwood, Hardwood, and Tunicate: Preparation-Structure-Film Performance Interrelation. *ACS Appl. Mater. Interfaces* **2017**, 13508.
(35) Cheng, Z.; Ye, H.; Cheng, F.; Li, H.; Ma, Y.; Zhang, Q.; Natan, A.; Mukhopadhyay, A.; Jiao, Y.; Li, Y.; Liu, Y.; Zhu, H. Tuning Chiral Nematic Pitch of Bioresourced Photonic Films via Coupling Organic Acid Hydrolysis. *Adv. Mater. Interfaces* **2019**, 1802010.
(36) Jonoobi, M.; Khazaeian, A.; Tahir, P. M.; Azry, S. S.; Oksman, K. Characteristics of Cellulose Nanofibers Isolated from Rubberwood and Empty Fruit Bunches of Oil Palm Using Chemo-Mechanical Process. *Cellulose* **2011**, 1085.
(37) Berzina-Cimdina, L.; Borodajenko, N. Research of Calcium Phosphates Using Fourier Transform Infrared Spectroscopy. In *Infrared Spectroscopy - Materials Science, Engineering and Technology*; BoD−Books on Demand, 2012; DOI: 10.5772/36942.
(38) Weiner, S.; Traub, W. Bone Structure: From Angstroms to Microns. *FASEB J.* **1992**, 879.
(39) Fathy, M.; Abdel Moghny, T.; Mousa, M. A.; El-Bellihi, A. H. A. A.; Awadallah, A. E. Absorption of Calcium Ions on Oxidized Graphene Sheets and Study Its Dynamic Behavior by Kinetic and Isothermal Models. *Appl. Nanosci.* **2016**, *6*, 1105−1117.
(40) Lee, H. L.; Chen, G. C.; Rowell, R. M. Thermal Properties of Wood Reacted with a Phosphorus Pentoxide-Amine System. *J. Appl. Polym. Sci.* **2004**, 2465.
(41) Bloebaum, R. D.; Skedros, J. G.; Vajda, E. G.; Bachus, K. N.; Constantz, B. R. Determining Mineral Content Variations in Bone Using Backscattered Electron Imaging. *Bone* **1997**, 485.
(42) Thula, T. T.; Rodriguez, D. E.; Lee, M. H.; Pendi, L.; Podschun, J.; Gower, L. B. In Vitro Mineralization of Dense Collagen Substrates: A Biomimetic Approach toward the Development of Bone-Graft Materials. *Acta Biomater.* **2011**, 3158.
(43) Jiao, K.; Niu, L. N.; Ma, C. F.; Huang, X. Q.; Pei, D. D.; Luo, T.; Huang, Q.; Chen, J. H.; Tay, F. R. Complementarity and Uncertainty in Intrafibrillar Mineralization of Collagen. *Adv. Funct. Mater.* **2016**, 6858.
(44) Gao, H.; Ji, B.; Jager, I. L.; Arzt, E.; Fratzl, P. Materials Become Insensitive to Flaws at Nanoscale: Lessons from Nature. *Proc. Natl. Acad. Sci. U. S. A.* **2003**, 5597.
(45) Weiner, S.; Wagner, H. D. THE MATERIAL BONE: Structure-Mechanical Function Relations. *Annu. Rev. Mater. Sci.* **1998**, 271.
(46) Li, Y.; Thula, T. T.; Jee, S.; Perkins, S. L.; Aparicio, C.; Douglas, E. P.; Gower, L. B. Biomimetic Mineralization of Woven Bone-like Nanocomposites: Role of Collagen Cross-Links. *Biomacromolecules* **2012**, *13*, 49−59.
(47) Farhadi-Khouzani, M.; Schütz, C.; Durak, G. M.; Fornell, J.; Sort, J.; Salazar-Alvarez, G.; Bergström, L.; Gebauer, D. A $CaCO_3$/Nanocellulose-Based Bioinspired Nacre-like Material. *J. Mater. Chem. A* **2017**, 16128.
(48) Liu, X.; Zhou, Y.; Pei, C. Mimetic Biomineralization Matrix Using Bacterial Cellulose Hydrogel and Egg White to Prepare Various Morphologies of CaCO3. *CrystEngComm* **2018**, 4536.
(49) Kuo, D.; Nishimura, T.; Kajiyama, S.; Kato, T. Bioinspired Environmentally Friendly Amorphous CaCO3-Based Transparent Composites Comprising Cellulose Nanofibers. *ACS Omega* **2018**, 12722.

DOI: 10.1021/acsami.9b09443
ACS Appl. Mater. Interfaces XXXX, XXX, XXX−XXX